



Universiteit
Leiden
The Netherlands

Probing gravity at cosmic scales

Peirone, S.

Citation

Peirone, S. (2020, October 6). *Probing gravity at cosmic scales. Casimir PhD Series*. Retrieved from <https://hdl.handle.net/1887/137440>

Version: Publisher's Version

License: [Licence agreement concerning inclusion of doctoral thesis in the Institutional Repository of the University of Leiden](#)

Downloaded from: <https://hdl.handle.net/1887/137440>

Note: To cite this publication please use the final published version (if applicable).

Cover Page



Universiteit Leiden



The handle <http://hdl.handle.net/1887/137440> holds various files of this Leiden University dissertation.

Author: Peirone, S.

Title: Probing gravity at cosmic scales

Issue Date: 2020-10-06

INTRODUCTION

1.1 THE STANDARD COSMOLOGICAL MODEL

In one sentence, we could summarise modern cosmology as the ambitious attempt to explain the physics of the entire Universe with a handful of parameters. As surprising as it may sound the latter approach has been to be remarkably successful in describing many observations through the six parameters of the so called standard cosmological model, or Λ CDM. This model is based on the theory of general relativity (GR) with the assumption of a cosmological constant Λ , being the simplest driver of the accelerated expansion of the Universe, and cold dark matter (CDM), responsible for structure formation. The most famous example of its success is perhaps the spectacular agreement of the Λ CDM predictions with the 2018 release of the cosmic microwave background (CMB) data from the Planck collaboration [1]. According to this model, the energy associated with Λ , to which we refer as dark energy (DE), amounts to about 68% of the total energy budget of the Universe while the CDM component contributes to 27%. This means that the total energy of all the visible matter only makes up 5% of the overall energy in the Universe, as shown in Figure 1.1.

It is then quite surprising that there is no theoretical explanation for the dark components of the standard model, i.e. for 95% of the current energy budget of the Universe. Regarding Λ , various attempts have been made to explain the cause of the cosmic acceleration, e.g. by considering a dark energy fluid or directly modifying the equations of GR. Furthermore, there are other unresolved observational puzzles within Λ CDM which motivate the quest for alternative cosmological

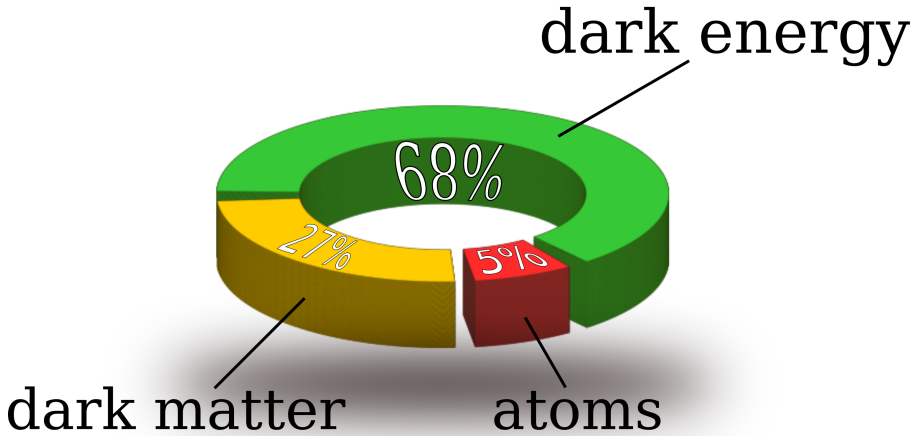


Figure 1.1: The Universe’s ingredients according to the Λ CDM model. Ordinary matter that makes up stars and galaxies contributes just 5% of the Universe’s energy inventory. Dark matter, which is detected indirectly by its gravitational influence on nearby matter, occupies 27%, while dark energy, a mysterious force thought to be responsible for accelerating the expansion of the Universe, accounts for 68%.

models. The first puzzle resides in the apparent discrepancy, referred to as “tension”, between the value of the expansion rate as inferred from high redshift experiments (for which a cosmological model must be assumed) and that which is extracted from local (model independent) measurements. In fact, from the 2018 Planck release we can measure the Hubble parameter today to be $H_0 = 67.4 \pm 0.5 \text{ kms}^{-1} \text{ Mpc}^{-1}$ [2], while the local determination from the Hubble Space Telescope (HST) is $H_0 = 74.03 \pm 1.42 \text{ kms}^{-1} \text{ Mpc}^{-1}$ [3]: a discrepancy with a significance of 4.4σ .

The tension is not so significant when analysing a supernova sample calibrated with the tip of the red giant branch, yielding $H_0 = 69.8 \pm 2.5 \text{ kms}^{-1} \text{ Mpc}^{-1}$ [4], while it is larger for the recent HoLiCOW quadrupole

lensed quasar measurement $H_0 = 73.3_{-1.8}^{+1.7} \text{ kms}^{-1} \text{ Mpc}^{-1}$ [5]. Surprisingly, both these measurements are falling between the CMB and the HST results, with uncertainties which are too large to shed some light on the puzzle.

Furthermore, a second inconsistency within the Λ CDM model dwells in the tension encoded by the derived parameter

$$S_8 = \sigma_8 \sqrt{\frac{\Omega_m}{0.3}} \quad (1.1)$$

with Ω_m being the matter density parameter and σ_8 the amplitude of the linear matter power spectrum at the scale of $8 h^{-1} \text{ Mpc}$, where $h = H_0/100 \text{ km s}^{-1} \text{ Mpc}^{-1}$. Once again the discrepancy appears between measurements at large and small scales, most noticeably the scales probed by the CMB and the small scale indicators of large scale structure (LSS), such as galaxy cluster counts, weak lensing (WL) and redshift space distortion (RDS) measurements [6], with LSS pointing towards a lower value of S_8 compared to CMB. In particular, if we measure S_8 from the combination of the Kilo Degree Surveys (KiDS) dataset and the Dark Energy Survey (DES) Year 1 release the tension with the Planck 2018 measurement reaches the 3.2σ level [7].

The coming decade will be key in order to assess if these tensions will survive the new generation of surveys, such as Euclid, DESI, SKA and LSST. In fact, one possible explanation could be that these inconsistencies of the Λ CDM model are just a statistical fluke, due to cosmic variance: the uncertainty intrinsic to the fact that we are observing finite patches in the sky. Another answer could be that one (or more) of the measurements are wrong: in this regard a lot of work has been done in order to quantify the effect of hidden systematics in the experiments [8–12], but, so far, none of the various effects considered seems to explain the large inconsistency between the datasets. Finally, the most intriguing scenario would be that the Λ CDM assumption is itself mistaken and the tensions are signalling that a new physical

model must be taken into account in order to describe the Universe from the smallest to the largest scales.

The aim of testing the robustness of GR on cosmological scales, together with the need to explain the physical nature of the cosmological constant, strongly motivates the quest for alternatives to the standard cosmological model, by either considering an exotic dark energy fluid component or by directly modifying Einstein's theory of gravity. This path of research goes under the name of dark energy or modified gravity cosmology and will be addressed in this work.

1.1.1 *Background cosmology*

Almost all theories of cosmology lay their foundations on the cosmological principle, which states that on sufficiently large scales the properties of the Universe are the same for all fundamental observers, i.e. the observers that are comoving with the expanding cosmological background. Being a principle, there is no way to prove its validity, but, so far, all experimental evidences justify this assumption. In particular, we know that on sufficiently large scales ($\gtrsim 100$ Mpc) the Universe appears isotropic and homogeneous. The most striking evidence of this is the isotropy of the cosmic microwave background radiation, whose photons are travelling to us from all directions in the sky with deviations in their wavelengths of order 10^{-5} . The most general metric compatible with this fact is the Friedmann-Lemaître-Robertson-Walker (FLRW) metric, defined by the line element

$$ds^2 = g_{\mu\nu} dx^\mu dx^\nu = -dt^2 + a^2(t) \left(\frac{dr^2}{1 - kr^2} + r^2 d^2\Omega \right), \quad (1.2)$$

where t is the cosmic time, r the radial coordinate on the spatial hypersurfaces, $d^2\Omega$ is the metric of a two-sphere and k indicates the curvature of the spatial slicing, which can be negatively curved, flat or positively curved. Finally, $a(t)$ is the scale factor which describes how

the length intervals on the spatial hypersurfaces contract or expand with t . Usually the scale factor is normalised in such a way that today $a_0 := a(t_0) = 1$. With this normalisation we have that $0 \leq a(t) \leq 1 \forall t$, meaning that the Universe is expanding with time. We know this since we can measure that the spectra of distant galaxies are redshifted: a spectral line with a restframe frequency ν_r is being observed with $\nu_o < \nu_r$. This phenomenon is due to the fact that, in an expanding universe, the electromagnetic waves are stretched along their paths to us. We can quantify this effect with the redshift z

$$z := \frac{\nu_r}{\nu_o} - 1 = \frac{a_0}{a(t')} - 1, \quad (1.3)$$

where t' is the time at which the signal was emitted. If we define the physical distance between two galaxies at a fixed cosmological distance r to be $d = a(t)r$ we can then infer the recession speed of a galaxy at a distance d from the observer to be

$$v = Hd, \quad (1.4)$$

where $H(t) = \dot{a}(t)/a(t)$ is the Hubble function and the dot represents the derivative with respect to t . The Hubble function is an essential quantity in cosmology which describes all the expansion history of the Universe by encoding the rate at which the scale factor changes. Finally, we can here introduce a new time coordinate known as conformal time

$$\tau(t) = \int_0^t \frac{dx}{a(x)}. \quad (1.5)$$

With this new coordinate the FLRW metric takes the form

$$ds^2 = \tilde{a}^2(\tau) \left(-d\tau^2 + \frac{dr^2}{1 - kr^2} + r^2 d^2\Omega \right), \quad (1.6)$$

where $\tilde{a}(\tau) = a(t(\tau))$. For simplicity, in the following we will neglect the tilde and simply write $a(\tau)$.

1.1.1.1 *In a FLRW Universe*

The dynamics of the FLRW metric is ruled by GR through the Einstein-Hilbert action

$$S = \frac{1}{2\kappa} \int d^4x \sqrt{-g} R + S_m, \quad (1.7)$$

where g is the determinant of the metric $g_{\mu\nu}$, R is the Ricci scalar, S_m is the action describing the dynamics of the matter fields. Finally $\kappa = 8\pi G$ where G is Newton's constant. Making use of the variational principle we can obtain the Einstein field equations

$$G_{\mu\nu} = \kappa T_{\mu\nu}, \quad (1.8)$$

where $G_{\mu\nu}$ is the Einstein tensor and $T_{\mu\nu}$ is the energy momentum tensor of the matter components. We can choose to describe the matter present in the Universe as a perfect fluid with rest frame energy density ρ and pressure p : in this case the energy momentum tensor can be written as

$$T_{\mu\nu} = (\rho + p)u_\mu u_\nu + p g_{\mu\nu}, \quad (1.9)$$

where u_μ is the four velocity of the perfect fluid. We can then insert the FLRW metric (1.2) and the energy momentum tensor (1.9) into (1.8), obtaining the Friedmann and acceleration equations:

$$H^2 = \frac{8\pi G}{3}\rho - \frac{k}{a^2}, \quad (1.10)$$

$$\frac{\ddot{a}}{a} = -\frac{4\pi G}{3}(\rho + 3p). \quad (1.11)$$

The diffeomorphism invariance of GR implies the continuity equation of the energy momentum tensor

$$\nabla_\mu T^{\mu\nu} = 0, \quad (1.12)$$

which, in case of perfect fluids can be written as

$$\dot{\rho} + 3H\rho(1 + w) = 0, \quad (1.13)$$

where $w := p/\rho$ is the equation of state parameter of the fluid. For each species i we can then solve eq (1.13) as

$$\rho_i \propto \exp\left(-3 \int \frac{da}{a}(1 + w_i)\right). \quad (1.14)$$

Therefore we have the following evolutions for the non relativistic matter (m , which contains both baryons and CDM) and radiation (r) components:

$$w_m = 0 \implies \rho_m \propto a^{-3}, \quad (1.15)$$

$$w_r = \frac{1}{3} \implies \rho_r \propto a^{-4}. \quad (1.16)$$

Along with these components another one is taken into account in the standard cosmological model: the cosmological constant Λ . This was originally introduced as a term $\Lambda g_{\mu\nu}$ into the Einstein equations (1.8), in order to obtain static solutions and then reintroduced when the measurements of the supernovae type Ia (SNIa) indicated that the expansion of the Universe is accelerating. From (1.11) we see that the late time acceleration is achieved if the Universe is dominated by an energy component with an equation of state parameter $w \leq -1/3$. In the case of the cosmological constant we have $w_\Lambda = -1$, which gives a component with constant energy density

$$\rho_\Lambda(a) = \rho_\Lambda(a_0) \quad \forall a \quad (1.17)$$

and described by the energy momentum tensor

$$T_{\mu\nu}^\Lambda = -\frac{\Lambda}{8\pi G} g_{\mu\nu}. \quad (1.18)$$

This means that we can think of the cosmological constant as a component of the Universe that serves the purpose of fuelling the late-time

accelerated expansion. If we want to explain the nature of the cosmological constant and to test its robustness on cosmological scales it is convenient to promote the vacuum to a fluid like component. Such fluid, which goes under the name of dynamical dark energy, is characterised by an equation of state parameter w_{DE} , which varies over time. The first step of DE research would be to detect deviations from $w_{\text{DE}} = -1$, in order to assess if DE can be identified by a cosmological constant or not [13].

In order to infer information from the observational data it is often useful to explore a broad class of DE models by assuming a dependence of w_{DE} over time, for example by means of a specific parametrization. One example would be to consider w_{DE} as a constant in time $w_{\text{DE}}(a) = w$ (w CDM cosmology) or adopt the Chevalier-Polarski-Linder (CPL) parametrization [14, 15]:

$$w_{\text{DE}}(a) = w_0 + w_a(1 - a), \quad (1.19)$$

which behaves as $w_{\text{DE}}(a) = w_0 + w_a$ at high redshift and as $w_{\text{DE}}(a) = w_0$ for $z = 0$. Such parametrizations are purely phenomenological and do not encode a clear physical meaning. They are, however, motivated by the behaviour of real physical models and they are necessary in order to achieve a complete characterization of dynamical DE when analysing cosmological data. For this reason they are an invaluable tool, but one has to remember that in most cases the results of the analysis will depend on the chosen parametrization.

1.1.2 Cosmological perturbations

As we mentioned in the previous section, the FLRW metric describes well the homogeneity and isotropy of the Universe at large scales ($\gtrsim 100$ Mpc). However, on smaller scales we know that the Universe is no longer homogeneous and isotropic. This is clear from the results

of both CMB experiments, where temperature fluctuations have been measured of the order of 10^{-5} , and LSS surveys, that are able to see a web of clustered matter, known as the cosmic web. In principle, the Einstein equations, which are highly non linear partial differential equations, would give the correct solution at all scales, but they cannot be solved analytically. However, the perturbations at large scales are small enough so that we can use perturbation theory. In the following we will then present the theory of linear order perturbations. We can start by considering the metric as

$$g_{\mu\nu} = \overline{g}_{\mu\nu} + \delta g_{\mu\nu} \quad (1.20)$$

where $\overline{g}_{\mu\nu}$ is the background FLRW metric and $\delta g_{\mu\nu}$ is the perturbation around it. When we perturb the gravitational field we can always decompose the contributions to the metric tensor in terms of irreducible representations of the rotation group. This means that the most generic form of $\delta g_{\mu\nu}$ will contain scalar, vector and tensor modes. These three types of perturbations will evolve independently. Since we want to study the evolution of cosmic structure, we will focus on the scalar perturbations. The most general form of the perturbed metric is

$$ds^2 = -(1 + 2\Phi)dt^2 + 2a\partial_i B dt dx^i + a^2[(1 - 2\Psi)\delta_{ij} + 2\partial_i \partial_j E] dx^i dx^j, \quad (1.21)$$

where Φ , Ψ , B , and E are functions of time and space. Thanks to gauge freedom we can reduce these four quantities to only two independent ones. Common gauge choices are the Newtonian gauge ($B = 0 = E$) and the synchronous gauge ($B = 0 = \Psi$). In the following we will work in the Newtonian gauge. In a similar way we can also perturb the energy momentum tensor (1.9) as

$$T_0^0 = -\bar{\rho}(1 + \delta), \quad (1.22)$$

$$T_j^i = (\bar{p} + \delta p)\delta_j^i + \pi_j^i, \quad (1.23)$$

$$T_i^0 = -T_0^i = (\bar{\rho} + \bar{p})v_i, \quad (1.24)$$

where bars denote background quantities, $\delta(t, \vec{x}) := \delta\rho/\bar{\rho}$ is the space dependent density contrast, $\delta p(t, \vec{x})$ is the pressure perturbation and v_i and π_j^i are the velocity and shear fields respectively. We can then insert the perturbed metric (1.21) and energy momentum tensor (1.22) into the Einstein equations (1.8) and expand the results up to first order in perturbations, obtaining the linearized Einstein equations:

0-0 component

$$k^2\Phi + 3\mathcal{H}(\Phi' + \mathcal{H}\Psi) = -\frac{8\pi Ga^2}{2}\bar{\rho}\delta, \quad (1.25)$$

0-i component

$$k^2(\Phi' + \mathcal{H}\Psi) = \frac{8\pi Ga^2}{2}(\bar{\rho} + \bar{p})ikv, \quad (1.26)$$

i-i component

$$\Phi'' + \mathcal{H}(\Psi' + 2\Phi') + (2\mathcal{H}' + \mathcal{H}^2)\Psi + \frac{8\pi G}{3}(\Phi - \Psi) = \frac{k^2 a^2}{2}\delta p,$$

i-j component

$$k^2(\Phi - \Psi) = 12\pi Ga^2(\bar{\rho} + \bar{p})\sigma, \quad (1.27)$$

where primes denote the derivative with respect to the conformal time τ and $\mathcal{H} = a'/a = aH$ is the conformal Hubble function. Finally, σ is the anisotropic stress

$$(\bar{\rho} + \bar{p})\sigma = -\left(\hat{\kappa}^j\hat{\kappa}_i - \frac{1}{3}\delta_i^j\right)\pi_j^i. \quad (1.28)$$

We can combine (1.25) and the anisotropy equation (1.27) and obtain the Poisson equation

$$k^2\Psi = -\frac{8\pi Ga^2}{2}\bar{\rho}\Delta, \quad (1.29)$$

where

$$\Delta := \bar{\rho}\delta + 3i\mathcal{H}(\bar{\rho} + \bar{p})\frac{v}{k}, \quad (1.30)$$

is the energy density in the synchronous gauge. The Poisson equation is a constraint equation, not dynamical, as it relates the metric potential Φ to the matter sources. Finally, in the presence of negligible shear the anisotropy equation states that the two gravitational potentials are equal

$$\Phi = \Psi. \quad (1.31)$$

We can then consider a single fluid and linearize the continuity equation (1.12), resulting in two independent equations

$$\delta' = -(1+w)(ikv - 3\Phi') - 3\mathcal{H} \left(\frac{\delta p}{\delta \rho} - w \right) \delta, \quad (1.32)$$

$$v' = -\mathcal{H}(1-3w)v - \frac{w'}{1+w}v - \frac{\delta p/\delta \rho}{1+w} ik\delta + ik\sigma - ik\Psi. \quad (1.33)$$

Usually, if we consider CDM, a collisionless non relativistic species, δ and v are sufficient to study the dynamic of the perturbed fluid, which rules the growth of structure during the matter era. We can then choose $w = 0$, a vanishing speed of sound $c_s^2 := \delta p/\delta \rho = 0$ and rewrite the linearized continuity equations as:

$$\delta' = -ikv + 3\Phi', \quad (1.34)$$

$$v' = -\mathcal{H}v - ik\Psi. \quad (1.35)$$

Finally we can combine these two equations with the anisotropy (1.27) and the Poisson (1.29) equations in order to obtain the master equation for linear structure formation

$$\delta'' + \mathcal{H}\delta' - \frac{3}{2}\mathcal{H}^2\delta = 0. \quad (1.36)$$

The solution of this equation gives CDM perturbations which evolve as $\propto t^{2/3}$ in the matter dominated era.

1.2 OBSERVABLES

In the previous section we described how the evolution of the Universe can be seen as a homogenous and isotropic background on top of which small inhomogeneities evolve linearly. Here we list some of the most important observables that have allowed us, in the past decades, to enhance our understanding of cosmology.

1.2.1 *Type Ia supernovae*

Type Ia supernovae are exploding stars with well calibrated light profiles. Since these objects can reach surprisingly high luminosities (as they can outshine an entire galaxy), they can be observed out to cosmological distances of several thousand megaparsecs [16]. Empirically it has been found that peak luminosities of SNIa are remarkably similar [17]. This means that they all have nearly identical absolute magnitude M , with small differences that can be taken into account if we consider the shape of their light curves. Because they all share the same absolute luminosity, SNIa are also known as standard candles. Since from Earth we can measure their apparent magnitude m , we can conclude that any difference that we measure in m from two different supernovae is due to the different distance that they have from us. The relation between the two magnitudes is given by

$$m = M + \log \left(\frac{d_L}{10 \text{ pc}} \right), \quad (1.37)$$

where d_L is the luminosity distance of the supernova. Observing $m - M$ allows us to measure the distance between us and the supernova, independently of its redshift. It is then possible to reconstruct the redshift-distance relation given by

$$d_L(z) = (1 + z) \int_0^z \frac{dz'}{H(z')}. \quad (1.38)$$

Since the two measurements are independent it is possible to use the standard candles to constrain the expansion history $H(z)$ (and, thus, the background evolution) of a specific cosmological model. An example of this is the Supernova Cosmology Project [18] and the High-Z Supernova Team [19], who were able to probe the redshift-distance relation for supernovae up to $z \sim 1.7$. Such measurements were able to determine that the Universe is currently undergoing a phase of accelerated expansion and the amount of dark energy (DE) needed to explain $\sim 70\%$ of the total energy budget.

1.2.2 Cosmic microwave background

At the early stages of its life the Universe was filled with a hot plasma of baryons and photons. When the temperature got sufficiently low the photons decoupled from the baryons and started to free-stream through the Universe. The decoupling occurred at $z_{\text{dec}} \simeq 1090$ and the free-streaming photons arrive directly at us generating the observed CMB sky. The small inhomogeneities that are present in the plasma are translated into fluctuations of the photon temperature, which we can observe today. We can treat such temperature fluctuations as a time-dependent background component plus the actual fluctuations, which depend on time, space and direction in the sky \hat{n}

$$T(\vec{x}, \hat{n}, \tau) = \bar{T}(\tau)[1 + \delta T(\vec{x}, \hat{n}, \tau)]. \quad (1.39)$$

Since we observe these fluctuations on a sky sphere, we are only interested in their angular dependence. We can then decompose them in spherical harmonics as:

$$\frac{\delta T(\vec{x}, \hat{n}, \tau)}{\bar{T}} = \sum_{\ell, m} a_{\ell m}(\vec{x}, \tau) Y_{\ell m}(\hat{n}), \quad (1.40)$$

where $\bar{T} = 2.725\text{K}$ is the average CMB temperature and $Y_{\ell m}$ are the spherical harmonics. The information coming from the CMB radiation

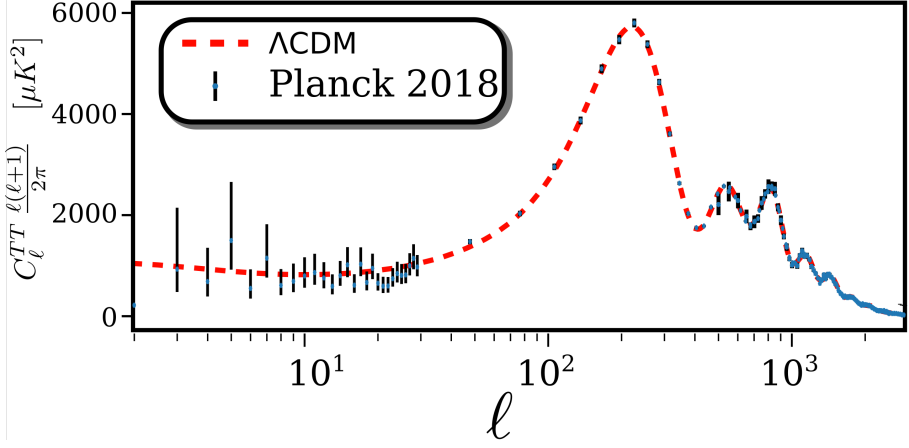


Figure 1.2: CMB Temperature-Temperature power spectrum C_ℓ^{TT} as a function of the multipole ℓ . In black we plot the data points from the Planck 2018 release [2] and in red the best fit obtained with the Λ CDM model.

is then encoded in the coefficients $a_{\ell m}$. We can usually assume that they are statistically isotropic, thus satisfying

$$\langle a_{\ell m} a_{\ell' m'}^* \rangle = \delta_{\ell \ell'} \delta_{m m'} C_\ell, \quad (1.41)$$

where C_ℓ is the angular power spectrum of the temperature anisotropies and the angular brackets denote the average over all the realizations of the random field. In figure 1.2 we show the value of the power spectrum for the temperature anisotropies as measured by the Planck collaboration [2] and its prediction by the Λ CDM model.

In order to measure C_ℓ one needs to extract the $2\ell + 1$ $a_{\ell m}$ coefficients from the sky map. The estimate of the power spectrum is then given by the average

$$\hat{C}_\ell = \sum_{m=-\ell}^{\ell} \frac{|a_{\ell m}|^2}{2\ell + 1}. \quad (1.42)$$

Since this is an average of finite independent terms, the result will recover the expectation value (C_ℓ) with limited precision. This means that there exists a fundamental uncertainty in how well we can measure the CMB power spectrum. This is known as the cosmic variance and is given by

$$\left(\frac{\Delta C_\ell}{C_\ell}\right) = \sqrt{\frac{2}{2\ell + 1}}, \quad (1.43)$$

meaning that this uncertainty increases for low values of the multipole ℓ .

1.2.3 Baryonic acoustic oscillations

In the epoch before decoupling, in the baryon-photon plasma, the baryons tend to cluster due to gravity, while the photons pressure prevents this from happening. The results of this interaction are acoustic oscillations throughout the whole cosmic plasma. When the baryons and photons decouple, the expansion of the plasma density waves is stopped and frozen into place. The fluctuations in the density of visible baryons, known as baryonic acoustic oscillations (BAO), are imprinted at a fixed scale, given by the maximum distance the acoustic waves were able to travel before decoupling. For this reason the BAO matter clustering provides a standard ruler for length scales in cosmology, analogous to the standard candle of supernovae. In fact, if one computes the correlation function between galaxy pairs, it is possible to notice an enhancement of the correlation for cosmic structures separated by the scale

$$r_s(z_{\text{drag}}) = \int_{z_{\text{drag}}}^{\infty} dz' \frac{c_s(z')}{H(z')}, \quad (1.44)$$

where $z_{\text{drag}} \approx 1020$ and c_s is the effective sound speed of the plasma.

In figure 1.3 we show the BAO effect in the galaxy-galaxy two-point correlation function $\zeta(r)$. We consider the best fit Λ CDM model

of figure 1.2 and a model without baryons ($\Omega_b = 0$). We compare these predictions with the data from the Sloan Digital Sky Survey (SDSS) sample [20]. As we can notice from the figure, the correlation function has a characteristic acoustic peak at a comoving scale $r \sim 100 h^{-1}$ Mpc, which is not present in the model without the baryonic component.

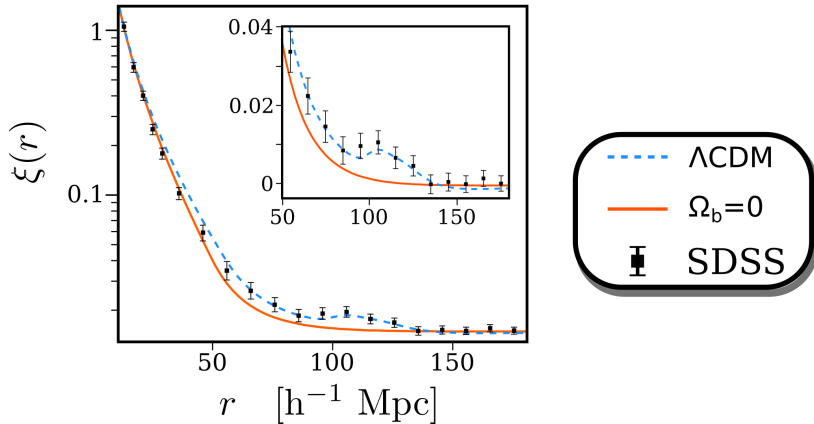


Figure 1.3: Large scale two points correlation as a function of the comoving distance between two galaxies. The data points are taken from the Sloan Digital Sky Survey (SDSS) sample [20]. The dashed blue line is the prediction for the Λ CDM model of figure 1.2, while the solid orange line represents a cosmological model without baryons ($\Omega_b = 0$). In the small panel we show an expanded view of the vertical axis.

1.2.4 Redshift space distortions

Accurate measurements of galaxy distances are rather difficult to obtain and their uncertainties become too large to be useful as one moves away from the local Universe. On the other hand, redshifts of galaxies are relatively easy to determine, but they are not a direct measure of distance, since the galaxy distribution in redshift space is distorted

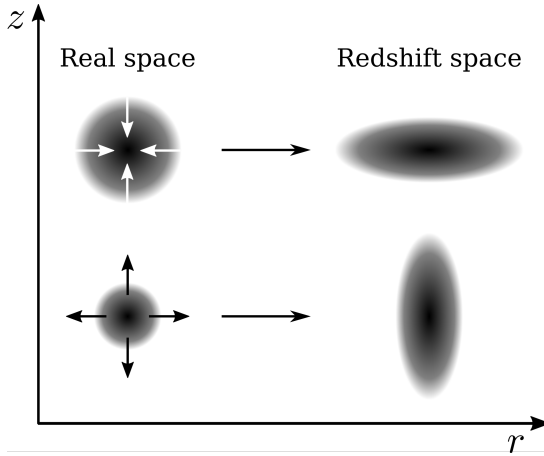


Figure 1.4: Illustration of the effect of peculiar velocities on RSD.

with respect to the distribution in physical space. In order to explain this we can go in the $z \ll 1$ limit and consider the relation

$$s := cz, \quad (1.45)$$

where s is the distance to a galaxy inferred through its redshift z and c is the speed of light. In this section distances are expressed in units of velocity. The physical distance would be

$$r := H_0 d, \quad (1.46)$$

where we have assumed the galaxy to be close enough such that a linearization of the Hubble relation applies. The two distances are then related by

$$s = r + v_r, \quad (1.47)$$

where $v_r = \vec{v} \cdot \hat{r}$ is the projection of the galaxy peculiar velocity along the line of sight.

From (1.47) we can see that the presence of peculiar velocities induces redshift space distortions (RSD). On one hand RSD complicate the interpretation of galaxy clustering, on the other hand they contain important information about the mass distribution in the Universe, since the peculiar velocities are caused exactly by the same distribution, which is correlated with the galaxy positions. In order to qualitatively analyse this effect we can imagine a simple spherical overdensity perturbation $\delta(r)$ within a radius r . Following the spherical collapse model, for a large value of r within which the overdensity is small the expansion of the mass shell is decelerated but its peculiar velocity is still too small to compensate for the Hubble expansion. In the redshift space the mass shell will thus appear squeezed along the line of sight. On the other hand, a completely virialized mass shell has peculiar velocities which exceed the Hubble expansion across its radius. The shell will then appear flattened along the line of sight, with the peculiarity that the nearer side has larger redshift distance than the farther side. These observational consequences of RSD are depicted in figure 1.4.

1.2.5 *Weak lensing*

Gravitational lensing is one of the most peculiar predictions of GR and it represents also the first experimental confirmation of Einstein's theory. In practice, it prescribes that the path of a light signal is deflected by the presence of a massive object. When the deflection is large we talk about strong gravitational lensing which is connected to the production of giant arcs and multiple images of one single object in the sky. Nevertheless, the majority of light coming towards us is in the weak lensing (WL) regime: when the electromagnetic signal travels nearby a massive distribution it gets slightly distorted. The net effect of this distortion is that we observe the shape of bright objects in the Universe, such as galaxies, to be different from how it is in reality. In figure 1.5 we show an exaggerated example of the deformation

caused by WL on galaxy shape. From the figure we can see that the intrinsic ellipticities of the galaxies are twisted in a coherent way. It is then possible to measure the ellipticity of the galaxies in the sky and construct a statistical estimate of their systematic alignment. Since the intrinsic orientation of the galaxies is expected to be random (apart from some intrinsic alignment contributions) any systematics in the alignment can be assumed to be due to the gravitational lensing. WL is thus a statistical measure which allows cosmologists to track the properties of the mass distributions in the Universe. The distortions of light can be described by the variation between the lensed position $\vec{\theta}$, at which we observe the signal, and the unaltered position of the source $\vec{\beta}$ as

$$\frac{\partial \theta_s^j}{\partial \theta^i} := \begin{pmatrix} -\kappa_{\text{wl}} - \gamma_1 & -\gamma_2 \\ -\gamma_2 & -\kappa_{\text{wl}} + \gamma_1 \end{pmatrix}, \quad (1.48)$$

where the convergence κ_{wl} describes the overall magnification effect, while γ_1 and γ_2 are the components of the shear and are connected to the distortion effect.

The gravitational lensing induced by the large structure of the Universe goes under the name of cosmic shear and it represents a distortion of only $\sim 0.1\%$. The cosmic shear is characterised by the shear correlation functions which quantify the mean product of the shear at two images as a function of the separation angle between the images. Since the shear has two components it is possible to define three different correlation functions which are computed by averaging over many pair of galaxies:

$$\xi_{++}(\Delta\theta) := \langle \gamma_+(\vec{\theta}) \gamma_+(\vec{\theta} + \vec{\Delta}\theta) \rangle, \quad (1.49)$$

$$\xi_{xx}(\Delta\theta) := \langle \gamma_x(\vec{\theta}) \gamma_x(\vec{\theta} + \vec{\Delta}\theta) \rangle, \quad (1.50)$$

$$\xi_{x+}(\Delta\theta) = \xi_{+x}(\Delta\theta) := \langle \gamma_x(\vec{\theta}) \gamma_+(\vec{\theta} + \vec{\Delta}\theta) \rangle, \quad (1.51)$$

$$(1.52)$$

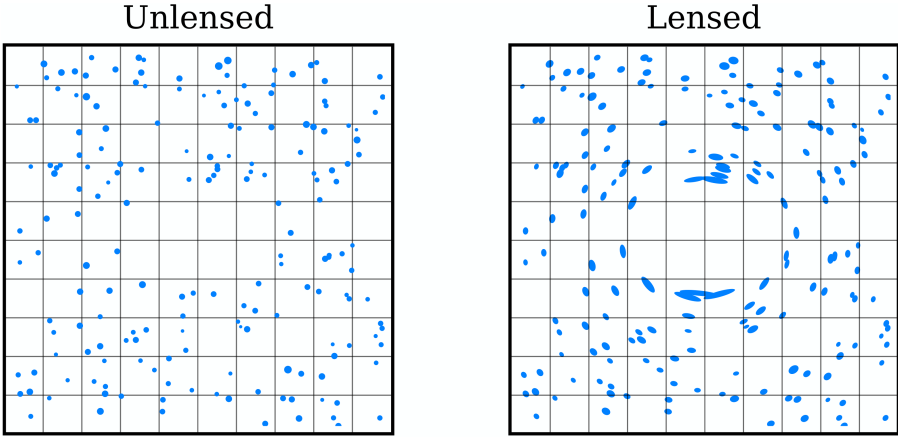


Figure 1.5: Illustration of the distortions caused by weak gravitational lensing.

where γ_+ is the shear component orthogonal to the separation angle $\Delta\vec{\theta}$ while γ_x is the component at 45° . Since the gravitational lensing does not allow the two different shear components to be correlated, checking that $\xi_{x+} = 0$ is a good test for systematic errors in the measurements.

Measures of these correlation functions directly constrain the cosmological parameters. The predictions of cosmic shear are particularly sensitive to a degenerate combination of the background matter density parameter (Ω_m) and the amplitude of the matter power spectrum (σ_8). In [21] it was shown that the amplitude correlation functions roughly scale with $S_8^{2.5}$, with

$$S_8 := \sigma_8 \sqrt{\frac{\Omega_m}{0.3}}. \quad (1.53)$$

As mentioned at the beginning of this chapter, there exists a tension of 3.2σ within the Λ CDM model on the value of S_8 measured from WL when compared to the Planck CMB results [7].

1.2.6 Local measurements of H_0

The local measurement of the value of the Hubble function today, H_0 , makes use of the cosmic distance ladder method [22], which allows to accurately measure distances from Earth to near and far galaxies. Using the Hubble Space Telescope (HST) [3], one can measure the distances to a class of pulsating stars called Cepheid variables, employing a basic tool of geometry called parallax: the change in the observer position (Earth revolution around the Sun) induces an apparent shift in the star's position. After calibrating the Cepheid's true brightness it is then possible to use it as cosmic yardsticks in order to measure distances to galaxies much farther away, for example to galaxies where both Cepheids and supernovae type Ia are hosted. It is then possible to use the Cepheids to measure the luminosity of the supernovae in each host galaxy. Going further in redshift (where only SN can be seen, but not Cepheids) one can compare the luminosity and brightness of the SN at a distance where the cosmological expansion can be observed. Comparing the redshift and the distances of those SN we can measure the local value of the expansion rate, H_0 .

The local measure of the Hubble constant today and the sound horizon ¹ observed from the CMB provide two absolute scales at opposite ends of the visible expansion history of the Universe. Comparing the two by means of a cosmological model provides a stringent test of the background cosmology. When assuming the standard cosmological model, Λ CDM, one finds a striking incompatibility between the Planck dataset and the local measurement of H_0 , of the order of 4.4σ [1, 3]. The root cause of this discrepancy is being actively investigated.

¹ the sound horizon, defined as $r_s = c_s(\tau^*)\tau^*$, where c_s is the sound speed, is the distance that a sound wave could have travelled before a time τ^* . The sound horizon is a fixed physical scale at the surface of last scattering to which the CMB power spectrum is particularly sensitive.

1.3 MODIFICATIONS OF GRAVITY

As anticipated in the previous section, the theoretical challenges of explaining cosmic acceleration and the tensions in the latest data are inspiring a great amount of theoretical work. The aim is to build a new theory of gravity which can, on one hand, replicate the numerous successes of Λ CDM and, on the other hand, solve the few tensions existing between high and low redshift datasets.

1.3.1 *The theory of Horndeski*

The theory of General Relativity is proven to be the unique theory of an interacting, massless, spin-2 field in four dimensions [23]. This means that any alternative theory of gravity should either go in the direction of considering a massive extension to GR, add an extra dynamical degrees of freedom, such as additional scalar-vector-tensor fields, or extend to higher dimensions.

A great number of models have been proposed in order to exploit one of the aforementioned alternatives. Although each of these approaches to modified gravity shows different and peculiar features, it can be proved that, at the scales which are relevant to cosmology, the low energy limit of such theories is often represented by GR with the addition of a dynamical scalar field. For this reason in this work we focus on such class of theories, known as scalar-tensor gravity. One of the most straightforward examples is given by Brans-Dicke gravity [24]. In this theory the additional dynamical scalar field ϕ has the physical effect of changing the effective gravitational constant from place to place in the spacetime. The action of Brans-Dicke gravity is:

$$S = \frac{1}{2\kappa} \int d^4x \sqrt{-g} \left(\phi R - \frac{\omega}{\phi} \nabla_\alpha \phi \nabla^\alpha \phi \right) + S_m, \quad (1.54)$$

where S_m is the action for the matter sector and ω is a dimensionless parameter known as the Brans-Dicke coupling constant. Gravity as described by Brans-Dicke theory is really well understood, both in the strong and in the weak field limit [25]. A number of different cosmological probes have been used in order to place constraints on Brans-Dicke theory. For example, using data from CMB it has been claimed that $\omega > 1000$ at 2σ [26].

The theory of Brans-Dicke is indeed a very special case of scalar-tensor theory. A more sophisticated example would be to consider a scalar field with a derivative self interaction given by a non standard kinetic term, as in the case of cubic galileon:

$$S = \frac{1}{2\kappa} \int d^4x \sqrt{-g} \left(R - c_2 \nabla_\alpha \phi \nabla^\alpha \phi - \frac{2c_3}{M^3} \square \phi \nabla_\alpha \phi \nabla^\alpha \phi \right) + S_m, \quad (1.55)$$

where c_2 and c_3 are dimensionless constants and $M^3 = m_0 H_0^2$, m_0 being the Planck mass. It is easy to prove that the theory given by 1.55 is invariant under the shift symmetry

$$\phi \longrightarrow b_\mu x^\mu + c, \quad (1.56)$$

which recalls of the Galilean symmetry, hence the name of the theory. Since 1.55 allows for self accelerating solutions even in the absence of a field potential [27], cubic galileon is a riveting theory if we want to answer questions about the nature of dark energy.

Following this example, we can exploit shift symmetry in order to build scalar-tensor theories with more complex interactions: this is the case of Covariant Galileons [28], whose action is given by

$$S = \int d^4x \sqrt{-g} \left[\frac{R}{16\pi G} - \frac{1}{2} \sum_{i=1}^5 c_i \mathcal{L}_i \right] + S_m, \quad (1.57)$$

with

$$\begin{aligned}
\mathcal{L}_1 &= M^3 \phi, \\
\mathcal{L}_2 &= \nabla_\mu \phi \nabla^\mu \phi, \\
\mathcal{L}_3 &= \frac{2}{M^3} \square \phi \nabla_\mu \phi \nabla^\mu \phi, \\
\mathcal{L}_4 &= \frac{1}{M^6} \nabla_\mu \phi \nabla^\mu \phi \left[2(\square \phi)^2 - 2(\nabla_\mu \nabla_\nu \phi)(\nabla^\mu \nabla^\nu \phi) - R \nabla_\mu \phi \nabla^\mu \phi / 2 \right], \\
\mathcal{L}_5 &= \frac{1}{M^9} \nabla_\mu \phi \nabla^\mu \phi \left[(\square \phi)^3 - 3(\square \phi)(\nabla_\mu \nabla_\nu \phi)(\nabla^\mu \nabla^\nu \phi) \right. \\
&\quad \left. + 2(\nabla_\mu \nabla^\nu \phi)(\nabla_\nu \nabla^\rho \phi)(\nabla_\rho \nabla^\mu \phi) - 6(\nabla_\mu \phi)(\nabla^\mu \nabla^\nu \phi)(\nabla^\rho \phi) G_{\nu\rho} \right].
\end{aligned}$$

It is possible to show that higher order Lagrangians are just total derivatives and hence they would not contribute to the equations of motion. In the quartic (\mathcal{L}_4) and quintic (\mathcal{L}_5) Lagrangians some terms are non minimally coupled to the metric: these are needed in order to retain that the scalar field equations are second order, which ensures the propagation of only one additional degree of freedom. Covariant Galileons have been extensively studied in cosmology [29–33] and they represents an interesting alternative to GR, which can alleviate the tensions between the cosmological datasets. Furthermore in [29] it has been proved the existence of tracking solutions in Covariant Galileon cosmologies, that finally approach a de Sitter fixed point, responsible for cosmic acceleration today.

The choice of invariance under shift symmetry is completely arbitrary and, in principle, one could ask if it is possible to write the most general scalar-tensor theory that includes all existing single field modifications of gravity as particular cases. It turns out that it is possible to do so and the action of the most general scalar-tensor theory with second order equations of motion, also known as the Horndeski class of theories [34–36], can be written as

$$S = \int d^4x \sqrt{-g} \left[\sum_{i=2}^5 \mathcal{L}_i + \mathcal{L}_m(g_{\mu\nu}, \chi_m) \right], \quad (1.58)$$

with

$$\begin{aligned}
\mathcal{L}_2 &= K(\phi, X), \\
\mathcal{L}_3 &= -G_3(\phi, X)\square\phi, \\
\mathcal{L}_4 &= G_4(\phi, X)R + G_{4X}[(\square\phi)^2 - (\nabla_\mu\nabla_\nu\phi)(\nabla^\mu\nabla^\nu\phi)], \\
\mathcal{L}_5 &= G_5(\phi, X)G_{\mu\nu}(\nabla^\mu\nabla^\nu\phi) \\
&\quad - \frac{1}{6}G_{5X}[(\square\phi)^3 - 3(\square\phi)(\nabla_\mu\nabla_\nu\phi)(\nabla^\mu\nabla^\nu\phi) \\
&\quad + 2(\nabla^\mu\nabla_\alpha\phi)(\nabla^\alpha\nabla_\beta\phi)(\nabla^\beta\nabla_\mu\phi)], \tag{1.59}
\end{aligned}$$

where K and G_i ($i = 3, 4, 5$) are functions of the scalar field ϕ and its kinetic energy $X = -\partial^\mu\phi\partial_\mu\phi/2$, R is the Ricci scalar, $G_{\mu\nu}$ is the Einstein tensor, G_{iX} and $G_{i\phi}$ denote the partial derivatives of G_i with respect to X and ϕ , respectively, and $\mathcal{L}_m(g_{\mu\nu}, \chi_m)$ is the Lagrangian for matter fields, collectively denoted with χ_m , minimally coupled to the metric $g_{\mu\nu}$. The constraint of having second order equations of motion is a sufficient condition in order to avoid Ostrogradsky instability [37], which is connected to an unstable Hamiltonian description of the theory. Nevertheless it is still possible to construct stable scalar-tensor theories with higher order equations of motion which contain a single propagating scalar degree of freedom. Such theories go under the name of beyond Horndeski or Gleyzes-Langlois-Piazza-Vernizzi (GLPV) [38, 39] extensions. Finally, GLPV theories were also extended to a larger class, known as Degenerate Higher Order Scalar Tensor (DHOST) theories [40, 41].

1.3.2 The effective field theory of dark energy

The wealth of theoretical models proposed in order to explain cosmic acceleration poses serious threats to the model selection in modern cosmology. If we decide to assess the preference of one model by looking at the observations we end up in a dramatic problem: how can

we efficiently discriminate among so many different gravity theories? Each one of them is characterised by a certain number of free parameters that have to be fitted against data, by solving the background and the perturbation equations. Practically, each DE model must be independently compared with Λ CDM in order to state which is the theory that better describes the data. The effective field theory (EFT) of dark energy simplifies this situation by implementing a unifying and model-independent approach. It is unifying in the sense that it incorporates many different models as particular cases: in fact it describes all the class of scalar-tensor theories up to GLPV. It is model independent since the operators of the EFT can be readily tested against observations without relying on any particular DE model.

The action of the EFT of DE is built in the unitary gauge. We can consider a foliation of spacetime by breaking the spacetime manifold into a family of three dimensional spacelike hypersurfaces parametrized by a function $t(x)$. Each hypersurface Σ_t is characterised by a timelike unit normal vector field n_μ and an induced spatial metric $h_{\mu\nu} = g_{\mu\nu} + n_\mu n_\nu$ (see Figure 1.6 for a pictorial representation). The unitary gauge is realised by choosing a time coordinate which is function of the scalar field $t = t(\phi)$: in such a way we have $\phi = \text{const.}$ on each hypersurface. This choice hides the explicit presence of the scalar field, since it is eaten by the metric components, and it breaks time diffeomorphism invariance. This last point has the effect that we are allowed to use generic functions of time in front of any terms in the Lagrangian. The timelike unit normal vector field to the hypersurface now reads:

$$n_\mu := -\frac{\partial_\mu \phi}{\sqrt{-(\partial\phi)^2}} \longrightarrow -\frac{\delta_\mu^0}{\sqrt{-g^{00}}}, \quad (1.60)$$

where we have used the fact that now ϕ is the new time coordinate and thus $\partial_\mu \phi = \delta_\mu^0$. Since, when building the DE action, we can contract any tensor with n_μ , we are left with terms with free upper 0 indexes, such as g^{00} or R^{00} . Furthermore, operators can also be built through

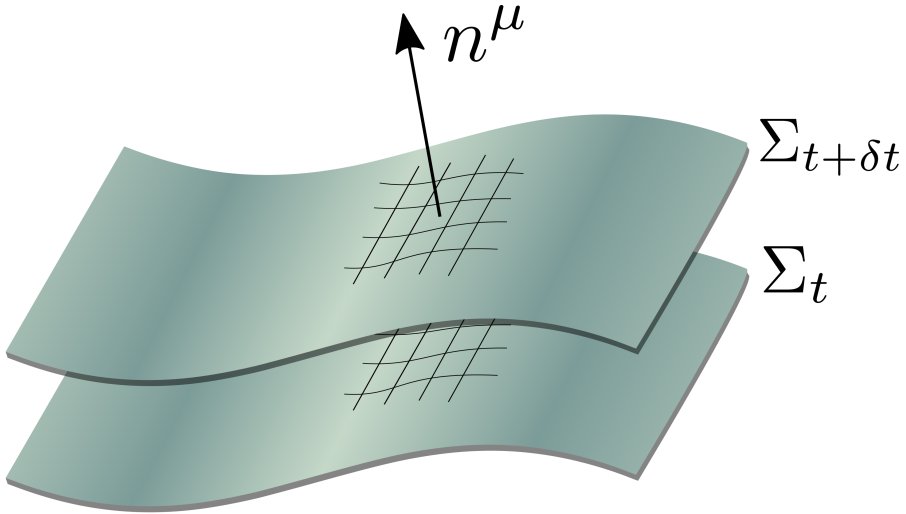


Figure 1.6: Pictorial representation of the foliation of spacetime given by the hypersurfaces Σ_t with the unit normal vector on the surface, n^μ .

covariant derivatives of the normal vector. For example, we can use their projection along Σ_t , named extrinsic curvature

$$K_{\mu\nu} := h_{\mu}^{\alpha} \nabla_{\alpha} n_{\nu}. \quad (1.61)$$

In this setup we can write the most general action up to quadratic order in perturbations [42–46]

$$\begin{aligned}
\mathcal{S} = & \int d^4x \sqrt{-g} m_0^2 \left\{ \frac{1}{2} [1 + \Omega(\tau)] R + \frac{\Lambda(\tau)}{m_0^2} - \frac{c(\tau)}{m_0^2} \delta g^{00} \right. \\
& + H_0^2 \frac{\gamma_1(\tau)}{2} (\delta g^{00})^2 - H_0 \frac{\gamma_2(\tau)}{2} \delta g^{00} \delta K - H_0^2 \frac{\gamma_3(\tau)}{2} (\delta K)^2 \\
& - H_0^2 \frac{\gamma_4(\tau)}{2} \delta K_j^i \delta K_i^j + \frac{\gamma_5(\tau)}{2} \delta g^{00} \delta \mathcal{R} \\
& \left. + \gamma_6(\tau) \partial^\mu (a^2 g^{00}) \partial_\mu (a^2 g^{00}) \right\} + \mathcal{S}_m [g_{\mu\nu}, \chi_m], \tag{1.62}
\end{aligned}$$

where $m_0^{-2} = 8\pi G$, and δg^{00} , δK_ν^μ , δK and $\delta R^{(3)}$ are, respectively, the perturbations of the time-time component of the metric, the extrinsic curvature and its trace and the three dimensional spatial Ricci scalar on the constant-time hypersurfaces. The action (1.62) is written in terms of the conformal time, τ . The functions $\Omega(\tau)$, $\Lambda(\tau)$ and $c(\tau)$ affect the evolution of the background and perturbations, with only two of them being independent as the third one can be derived using the Friedmann equations. The remaining functions, γ_i , $i = 1, \dots, 6$, control the evolution of perturbations.

All of these time dependent functions are known as *EFT functions* and they are essential for this framework to be unifying as well as model independent. In fact, on one hand, it is possible to specify a specific time dependence of the EFT functions, e.g. through some parameterizations, and to test the effect of each operator on the phenomenology. On the other hand, they can be expressed in terms of the functions appearing in the Horndeski Lagrangian (1.59) [45], in order to reproduce the phenomenology of a given scalar-tensor theory. We refer to this process as *mapping procedure*.

As previously stated, action (1.62) can reproduce the phenomenology of any GLPV theory. In the case of mapping to Horndeski theory, which is a subset of GLPV, the following constraint applies

$$\begin{aligned}
\gamma_4 &= -\gamma_3, \\
\gamma_5 &= \frac{\gamma_3}{2}, \\
\gamma_6 &= 0.
\end{aligned} \tag{1.63}$$

1.3.3 The α -basis

An equivalent and alternative way of parameterizing the EFT action for linear perturbations around a given FLRW background in Horndeski models is based on the following action for linear perturbations [47–50]:

$$\begin{aligned}
S &= \int d^4x a^3 \frac{M_*^2}{2} \left\{ \delta K_i^j \delta K_j^i - \delta K^2 + R \delta N \right. \\
&\quad + (1 + \alpha_T) \delta_2 \left(\sqrt{h} R / a^3 \right) + \alpha_K H^2 \delta N^2 \\
&\quad \left. + 4\alpha_B H \delta K \delta N \right\} + S_m[g_{\mu\nu}, \chi_m],
\end{aligned} \tag{1.64}$$

where N is the lapse function. The role of the EFT functions is here covered by five functions of time: the Hubble rate H , the generalized Planck mass M_* , the gravity wave speed excess α_T , the *kineticity* α_K , and the *braiding* α_B [47]. One also defines a derived function, α_M , which quantifies the running of the Planck mass. The relations between the functions in the two EFT approaches is given by

$$\begin{aligned}
\Omega(a) &= -1 + (1 + \alpha_T) \frac{M_*^2}{m_0^2}, \\
\gamma_1(a) &= \frac{1}{4a^2 H_0^2 m_0^2} [\alpha_K M_*^2 \mathcal{H}^2 - 2a^2 c], \\
\gamma_2(a) &= -\frac{\mathcal{H}}{aH_0} \left[\alpha_B \frac{M_*^2}{m_0^2} + \Omega' \right], \\
\gamma_3(a) &= -\alpha_T \frac{M_*^2}{m_0^2}, \\
\gamma_4(a) &= -\gamma_3, \\
\gamma_5(a) &= \frac{\gamma_3}{2} \\
\gamma_6(a) &= 0.
\end{aligned} \tag{1.65}$$

We emphasize a key difference between the two EFT descriptions. In the first, the expansion history is derived, given the EFT functions. In the second approach, $H(a)$ is treated as one of the independent functions that needs to be provided. This distinction is important when it comes to sampling the viable solutions of Horndeski theories, as it amounts to a different choice of priors.

1.3.4 EFTCAMB and stability conditions

In order to study the phenomenology of scalar-tensor modifications of GR, the EFT of DE approach has been implemented in the public Einstein-Boltzmann solver CAMB (Code for the Anisotropies in the Microwave Background) [51]. The resulting code is known as EFTCAMB [52, 53]. Based on the EFT of DE approach, EFTCAMB can be employed for different purposes. The code can evolve the full set of linear scalar perturbation equations of any single field scalar-tensor theory, up to GLPV, once a mapping between the model and the EFT of DE is provided

(mapping approach). Furthermore, it allows for agnostic investigation of gravity on cosmological scales, for example by specifying a preferred parametrization for the evolution of the EFT functions (pure EFT approach).

One of the strengths of EFTCAMB is that it does not rely on any quasi static (QS) approximation. When fitting data one usually focuses on sub horizon scales and neglects the time derivatives of the scalar field and gravitational potential compared to their spatial gradient: this is the QS approximation. On one hand the employment of the QS regime simplifies both the theoretical and the numerical setup, still giving a good description of the physics at sub horizon scales [54], on the other it might lose some dynamics at scales and redshifts that are relevant for upcoming surveys [55, 56].

The reliability of EFTCAMB has been tested against several existing Einstein-Boltzmann solvers, showing a remarkable agreement [57].

Furthermore, the code has been interfaced with a modified version of the Monte Carlo Markov Chain (MCMC) integrator CosmoMC [58], which allows to explore and constrain the parameter space of modified gravity models by performing a fit to cosmological data. When performing parameter estimation for a DE model, one needs to verify that the sampled point in the parameter space satisfies specific criteria of theoretical viability. We refer to these criteria as stability conditions and they mainly include the avoidance of the following three classes of instability:

- Ghost instability: the ghost corresponds to the presence of fields with negative energy or negative norm, typically connected to a wrong sign in the kinetic term. This leads to an unstable vacuum as the spontaneous particle production process would cost zero energy and it would have infinite decay rate.
- Gradient instability: this instability is due to an imaginary speed of sound of the scalar field, which translates into a catastrophic

growth of DE perturbation modes. Since this instability has an intrinsic timescale, in cosmology we say that a model is safe from gradient instability when this timescale does not exceed the timescale of the Universe, given by the Hubble time.

- Tachyon instability: it is a large-scale instability which is sourced by a mass term with wrong sign, which in turn is related to the unboundedness of the Hamiltonian from below [59, 60].

Imposing such stability conditions during a MCMC analysis guarantees not only that the dynamical equations are mathematically consistent and can be meaningfully solved, but also that the underlying theory is physically acceptable. This is true when considering a specific DE model, but even more when performing analysis in the pure EFT approach, where the choice of the time dependence of the EFT functions is completely arbitrary. The imposition of stability conditions in the MCMC algorithms divides the parameter space of a theory into patches, in some of them the theory is stable while in others instabilities occur. This partitioning of the parameter space could, in principle, alter some important statistical properties of the MCMC. In order to avoid this issue, the stability conditions have been implemented as stability priors: the Monte Carlo step is rejected whenever it falls in one of the unstable patches. Since the stability priors are well motivated from the theoretical point of view, and they are a natural requirement for the DE model (or parametrization) considered, they represent the degree of belief in viable underlying theory encoded in the EFT framework.

1.4 CONSTRAINTS FROM GRAVITY WAVES

The detection of the gravitational wave (GW) event GW₁₇₀₈₁₇ and the associated gamma-ray bursts GRB_{170817A} from a neutron star

merger [61–63] has put stringent constraints on the difference between the speed of light ($c = 1$) and gravitational waves

$$-3 \times 10^{-15} < c_T - 1 < +7 \times 10^{-16}. \quad (1.66)$$

This has a significant implication for modified gravity models, in particular scalar-tensor theories [64–77]. In the case of Horndeski the surviving viable action includes a reduced number of EFT functions. In particular, the quintic order Lagrangian is vanishing ($G_5 = 0$) and the quartic order reduces to a general function of the scalar field alone ($G_{4,X} = 0$). However, it is still possible to recover the quintic order once we move to GLPV theories, as it will be shown in chapter 4. Although such observation had a profound impact on the modified gravity community, possibly ruling out a large class of theories, it is worth noticing that the extent to which this bound applies to the EFT of DE is still under debate. In fact, as pointed out in [78], the energy scales detected by the LIGO collaboration lie very close to the typical cutoff of many DE models.

1.5 THIS THESIS

The primary aim of this thesis is shedding light on the nature of dark energy and the theory of gravity on cosmological scales. We do so by presenting different approaches that we can adopt when we want to study the cosmology of modified gravity models. Specifically:

- Chapter 2 studies the impact of general conditions of theoretical stability and cosmological viability on the analysis of dynamical DE models with cosmological data. Recently, the KiDS collaboration has found a mild preference for a CPL DE model over Λ CDM when combining their data with Planck [79]. Interestingly, this model has been found to alleviate the tension on the S_8 parameter, between CMB and WL measurements. In chapter 2, we use the powerful stability check which is built-in in the EFTCAMB

code, in order to verify if such results are compatible with a stable theoretical description, i.e. a quintessence field which does not develop ghost instabilities. This chapter is based on Ref. [80].

- Chapter 3 describes the building blocks that are needed in order to obtain meaningful theoretical priors for cosmological analyses of DE models. When comparing the theory predictions with data a convenient approach is to look at phenomenological departures at the level of linear perturbations equations. This approach is an alternative to the EFT of DE framework: while the former is more directly connected to the observation, the latter is more prone to keep the connection between phenomenology and the underlying theory of gravity. By building a bridge between the two approaches it is then possible to connect a single EFT operator to a specific phenomenological feature. On the other hand, through the EFT, it is possible to impose conditions of theoretical stability and study their effects on the model phenomenology. This is done by creating numerical samples of theoretically viable Horndeski models, studying the typical trends for their phenomenology and computing theoretical priors that can be exploited in a non parametric reconstruction from data. This chapter is based on Refs. [81, 82].
- Chapter 4 shows the full study of a specific dark energy model in the framework of Gleyzes-Langlois-Piazza-Vernizzi theories, which predicts a speed of gravity waves compatible with the observational constraints. We present the signatures of the model on some relevant observables. In this model, we show that the Planck cosmic microwave background data, combined with datasets of baryon acoustic oscillations, supernovae type Ia, and redshift space distortions, give a tight upper bound on the beyond Horndeski parameter α_H . Finally, we make use of specific model selection criteria in order to assess the model preference with respect

to Λ CDM. We find that the model considered fits the data better than Λ CDM according to the χ^2 statistics, yet the deviance information criterion (DIC) slightly favours the latter. However, we show that the Horndeski limit of the model, known as Galileon ghost condensate, is preferred over the standard model of cosmology by the data. This chapter is based on Refs. [83, 84].

